Comparing the Effects of Three MRI RF Sequences on Ultrasonic Motors

P. Shokrollahi[1], J.M. Drake[1,2] and A.A. Goldenberg[1]

[1] University of Toronto, Institute of Biomaterials and Biomedical Engineering, Toronto, Canada
[2] Division of Neurosurgery, the Hospital for Sick Children, Toronto, Canada

Abstract— **Obtaining accurate force and kinesthetic information produced by actuators is necessary for the success of robot-assistive surgical operations. Access to such information is not readily possible in MR environments due to the effects of giant static and gradient magnetic fields. The goal of this study is to quantify the effects of MRI on the behavior of ultrasonic motors (USMs), while performing bone biopsies on pediatric surgery. In this study, the effects of three sequences (FFE, balanced FFE, and ultra-fast spin echo, SSH-TSE) were considered on the torque generated by a USM, transferred as an axial force by our implemented robot and measured by our developed force feedback system. Different sequences show different effects on the generated axial force while the motor rotates in different directions**

Keywords— **Ultrasonic motor, robotic surgery, force, MRI-compatibility, MRI-sequence.**

I. Introduction

Magnetic resonance imaging (MRI) can be used not only in the diagnosis of many diseases [1], but also in their treatment, through the use of robot-assistive tools. Modern surgical robots can perform various operations on a wide range of tissues; for example, P-robot implemented for thermal ablation, radioactive seed implants (brachytherapy), and biopsy for prostate interventions [2]. The motorized manipulator was developed for performing microwave thermo-coagulation on liver tumors [3]. The real time MR image-guided robot was designed to assist surgeons in both puncture and laparoscopic surgeries [4]. Furthermore, NeuroArm has been implemented to cut, suture, biopsy, electrocauterize, aspirate, and irrigate [5].

The goal of these developments is to enhance the capabilities of surgeons through enriching their visual capabilities with MRI as well as to help them to gain greater dexterity [6].

Using MRI does impose severe restrictions on plans to construct mechatronic devices that must function inside or in proximity to the scanner. Conventional electromagnetic actuators are no longer valid, and only non-magnetic materials can be used. In some of the cases, MR imaging of the patient is impossible due to large magnetic coupling effects such as torque, force, or heating problems [7].

However, using non-magnetic materials decreases the rigidity of the system and causes mechanical problems. These types of robot are not able to provide large forces, and they suffer from the vibration problems during the scanning time, in which the acoustic knocks the patient table. On the other hand, electronics, the important parts of the controlling systems of the robots, are restricted to being used in the MR environment. Nonetheless, employing these components is necessary for designing accurate actuators.

In fact, among the various categories of available actuators, only four can be utilized in the vicinity of the scanner: ultrasonic, hydraulic, pneumatic, and remote-manual actuators [8].

Ultrasonic motors (USMs) are commonly employed for designing MRI-compatible surgical robots as they have the advantages of high torque/size ratio, small size, and short response time. USMs do not operate by magnetism. Instead, the travelling wave of the stator produced by piezoelectric material moves the rotor by using friction force. According to a well-known principle, the rotor moves by a torque caused by frictional force to the elliptically vibrating surface of a stator [9]. However, the output torque generated by the motor is not linearly dependent on the inputs.

The non-linearity of the input-output characteristics causes difficulties in detecting the motors' output behavior. Various models of travelling wave USM have been created. Sun *et al.* introduced an analytical-mechanical model for vibrations of the stator, and the contact between the stator and the rotor [10] Hagood *et al*. used the Rayleigh-Ritz method to model the traveling wave dynamics of the stator [11]. Frangi *et al.* proposed a 3-dimensional model for dynamic analyses of the stator alone to find the resonant frequencies and to replicate the travelling waves [12].

All these evaluations concern the effects of the motor on the MR-images, but a general model considering the effects of MR on the motor's output behavior has not been developed. Quantifying the behavior of the USM inside the MRI can lead to accurate control of the motor, which can result in a successful operation using robotic surgical tools and MRI simultaneously. This can reduce the time of the procedure and consequently decrease the cost of hospitalization, as well as provide more dexterity to the surgeons. The model can harness the output of the motor and can be used for developing MRI-compatible haptic devices.

D.A. Jaffray (ed.), *World Congress on Medical Physics and Biomedical Engineering, June 7-12, 2015, Toronto, Canada*,
IFMBE Proceedings 51, DOI: 10.1007/978-3-319-19387-8_207

Due to the complex and nonlinear characteristics of USMs, a motor's output torque cannot be readily calculated from input values. Modeling USM output behavior is therefore required. However, an MRI system's effects – such as vibration disturbance and temperature shift – on USM performance have not, to date, been adequately evaluated. In addition, developing a model of motor output with a time-varying load is valuable because the inhomogeneities of a bone or soft tissue while undergoing penetration by a drill or needle can be considered a time-varying load.

The nonlinearities of the rotor-stator behavior have not been modeled, while the motor is operating in the MRI. In addition, the high static and gradient magnetic field has more effects on motor nonlinear behavior. The motor creates artifacts when it is too close to the region being imaged. One of the ways frequently employed to avoid image artifacts created by EM noise emissions and conductive materials is to shield and separate the actuators from the imaging volume, at a certain distance [2].

In addition, conventional sensors cannot be used in MRI, and MRI-compatible sensors are required for measuring the entities, including force. Utilizing an MRI-compatible force feedback system can help to track USM output behavior. Similar to USM motors, not all types of force sensors are MRI-compatible. Specific MRI-compatible polymers such as piezoresistive composites can be utilized to develop pressure transducers or force sensors [13] [14].

The ultimate goal of this research is to model the motor's nonlinearities inside the MR environment. In this paper we show the effects of three different MRI sequences on the force generated by the USM.

II. Methodology

A. Robot and force sensor system development

A one degree-of-freedom (1DoF) robot (Fig. 1) was designed to measure the axial force generated by the USM motor (PUMR40, PiezoElectric Technology Co., Ltd., South Korea). To do so, the torque produced by the motor was transferred to an axial force using a screw system.

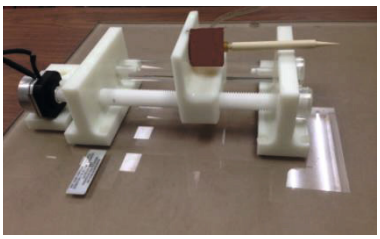

Fig. 1 The MRI-compatible 1 DoF robot

To measure and control the axial force, we developed our own MRI-compatible force feedback system utilizing a piezoresistive sensor (Tekscan Flexiforce sensor, A201).

In order to avoid compatibility issues, MR-compatible polymers such as Ultem, Delrin, and high-density polyethylene were used to build the robot. The mechanical properties of these materials such as stiffness, tensile strength, and shear strength were considered. These properties were selected so that the materials would be able to tolerate the high forces required for the bone biopsy.

We measured and analyzed the drilling force on swine and hen bones in time and frequency domains. We concluded that the maximum axial force that can be applied for bone drilling is about 100N.

The axial force was measured while the needle was freely moving forward and backward outside the MRI, for both forward and reverse directions. A calibration curve was used to evaluate force from the corresponding output voltage. The force values were measured when the motor was running CCW and then CW for 4s each.

B. MR image acquisition

The robot was placed near the isocentre in a 3T Achieva scanner (Philips Healthcare, Best, NL). The robot controllers and acquisition systems were located in the control room. The magnitude and phase images were acquired utilizing three sequences: FFE, b-FFE, and TSE (TE = 72 ms, TR = 4.0 s, FOV = 200 mm, in-plane voxel size = 1.5 mm, slice thickness = 5 mm (Fig. 2)) [15].

In order to acquire both transverse and coronal images, a Philips mineral oil phantom was located at the side of the USM motors. The axial applied force was generated by driving the phantom needle mounted on top of the sensor. The applied force was measured both inside and outside the MR environment. The acquired data was processed for further analysis using MATLAB 2013b.

III. RESULTS

A. Force measurements

Figure 2 shows the force applied to the needle at no load, while the motor was rotating CCW (the first step function) and then CW (the second step function) while scanning coronal images with balanced FFE sequence.

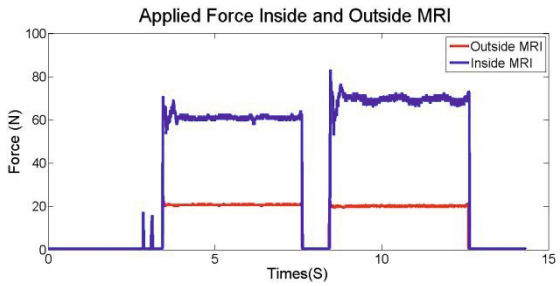

Fig. 2 Applied force inside and outside MRI with balanced FFE Sequence

Figure 3 shows the force applied to the needle at no load, while the motor was rotating CCW and then CW while scanning coronal images with ultra-fast spin echo, SSH-TSE sequence.

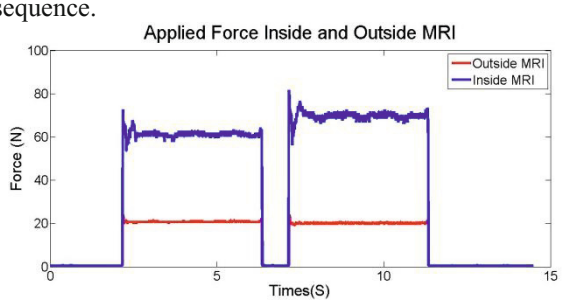

Fig. 3 Applied force inside and outside MRI with SSH-TSE sequence

Figure 4 shows the similar experience during coronal scanning of the motor with a FFE sequence.

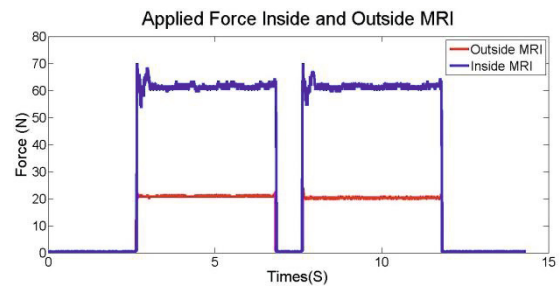

Fig. 4 Applied force inside and outside MRI with FFE Sequence

IV. DISCUSSION

If a command such as the motion command was sent to the motor during the pre-scanning time, in which the MR gradient coils were being prepared to perform the imaging, the command was not received by the motor and the motor did not move. Therefore, the commands had to be sent after the scanner began running and the knocking of RF coils had started.

It is important to note that if the pause time between two directional rotations (CCW and CW) was less than a certain interval, the commands were not received by the motor and the motor was halted. Shielding strategy of the motor cables may improve this minimum pause time.

The amplitude of the sensor's output voltages, which are converted to force in the figures, changed with the same ratio when compared inside and outside the MRI. For forward motion for both balanced FFE and SSH-TSE sequences, the force inside the MRI was three times higher than it was outside the MRI. For reverse motion on these sequences, the force inside the MRI was three and half times more than outside. In the FFE sequence, the force was almost three times more outside the MRI than inside for both directions.

The motor was tested 15 times for no-load conditions. The reason for the difference inside and outside the MRI is that the MRI sequence affects the rotation of the motor shaft and other metallic parts of the motor. In addition, a higher induction voltage is possible while the motor is running inside the MRI than when it is outside.

V. CONCLUSIONS

A model that can quantify the effects of MRI on the output of USMs is required. The model can be used for developing a generic surgical tool. Here, the goal was to model the behavior of these devices for bone drilling in pediatric surgeries.

The applied force generated by the ultrasonic motor was tested inside and outside an MRI. The effects of three sequences were considered on the axial force originated from a USM, applied to a phantom needle through our designed robot and force feedback system.

The sequences affect the motor output differently. Different axial forces were generated while the motor rotated in different orientations. The applied force inside the MRI was larger than that of outside the MRI.

In conclusion, quantifying the motor behavior in MRIhelps optimal design of mechanical systems as well as developing suitable image sequences that can be utilized in MRI-compatible robotic surgeries.

ACKNOWLEDGMENT

This work was financially supported by A. A. Goldenberg's NSERC CHRP Grant 385860-10. Also, we would like to thank Adam Waspe and Wendong Wang for their support.

CONFLICT OF INTEREST

The authors declare that they have no conflict of interest.

REFERENCES

1. Luechinger R, Firat Duru, M B et al. (2001) Force and Torque Effects of a 1.5 Tesla MRI Scanner on Cardiac Pacemakers and ICDs. Pace 24 (2): 199-205
2. Goldenberg, A A, Trachtenberg, J et al. (2010) Robot-assisted MRI-guided prostatic interventions. Robotica 28 (2): 215-234
3. Morikawa, S, Shigeyuki N et al. (2009) Preliminary clinical experiences of a motorized manipulator for magnetic resonance image–guided microwave coagulation therapy of liver tumors. Am J Surg 198 (3): 340-347
4. Hashizume, M, Takefumi, Y et al. (2008) New real-time MR image-guided surgical robotic system for minimally invasive precision surgery. Int J Comput Assist Radiol Surg 2 (6): 317-325
5. Sutherland, G R, Latour I (2008) An Image-Guided Magnetic Resonance-Compatible Surgical Robot. Neurosurgery 62 (2): 286-293.
6. Elhawary, H, Zivanovic, A et al. (2006) A review of magnetic resonance imaging compatible manipulators in surgery. Proc. Inst. Mech Eng H J Eng Med 220(3): 413-424
7. Luechinger, R, Boesiger, P et al. (2007). Safety evaluation of large external fixation clamps and frames in a magnetic resonance environment. J Biomed Mater Res B Appl Biomaterials 82(1): 17-22.
8. Yang, B, Tan, U X et al. (2011) Design and control of a 1-DOF MRI-compatible pneumatically actuated robot with long transmission lines. IEEE/ASME Trans Mechatronics 16(6): 1040-1048.
9. Kumada, A (1985) A piezoelectric ultrasonic motor. Japanese J Appl Physics 24(S2), 71-83 DOI 10.1177/1045389X9500600110
10. Sun, D, Liu, J et al. (2002) Modeling and performance evaluation of traveling-wave piezoelectric ultrasonic motors with analytical method. Sensors and Actuators A Physical 100(1): 84-93
11. Hagood, N W, McFarland, A J (1995) Modeling of a piezoelectric rotary ultrasonic motor. IEEE Trans Ultrason Ferroelectr Freq Control 42(2): 210-224
12. Frangi, A, Corigliano, A et al. (2005) Finite element modelling of a rotating piezoelectric ultrasonic motor. Ultrasonics 43(9): 747-755
13. Wang, L, Li, Y (2013) A review for conductive polymer piezoresistive composites and a development of a compliant pressure transducer. IEEE Trans Instrum Meas 62(2): 495-502
14. Beebe, D J, Hsieh, A S et al. (1995) A silicon force sensor for robotics and medicine. Sensors and Actuators A Physical 50(1): 55-65
15. Armitage, P, Berry, G, Matthews, J N (2002). Statistical methods in medical research. Blackwell Science Ltd. Malden, Massachusetts

Author: Peyman Shokrollahi
Institute: University of Toronto
Street: 11 King's College Road
City: Toronto
Country: Canada
Email: peyman.shokrollahi@mail.utoronto.ca